Lateral distribution of depth average velocity & boundary shear stress in a gravel bed open channel flow

Prateek Kumar Singh, Sumit Banerjee, Bandita Naik, Arun Kumar & Khisanjit Kumar Khatua

Taylor & Francis
Taylor & Francis Group

Check for updates
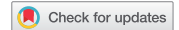
Lateral distribution of depth average velocity & boundary shear stress in a gravel bed open channel flow

Prateek Kumar Singh [a], Sumit Banerjee[b], Bandita Naik[c], Arun Kumar[a] and Khisanjit Kumar Khatua [a]

[a]Department of Civil Engineering, National Institute of Technology, Rourkela, India; [b]Department of Civil Engineering, B A College of Engineering &Technology, Jamshedpur, India; [c]Department of Civil Engineering, BPUT College, Rourkela, India

ABSTRACT

Gravel bed flow is so generic condition that its study becomes fascinating as well as critical to apprehend flow characteristic. In this particular study, no bed load movement was maintained using grains of 13.5 mm (D_{50} value) characterised as no load condition. Depth Average Velocity (DAV) and the Boundary Shear Stress (BSS) has been experimentally estimated for five different depths for the prevailing no load condition. Furthermore, the distribution of streamwise depth-averaged velocity and boundary shear stress at different flow depths of gravel bed are also calculated using different hydraulic software packages such as CES & ANSYS FLUENT. These numerical simulation results have shown reasonably good agreement with experimental data over main channel in inbank flow. Finally, results obtained are corroborated through error analysis. The overall idea of this study was to understand flow characteristic and behaviour of gravel bed having inbank flow through experimental and numerical simulation techniques.

1. Introduction

Open channel flows are free surface which may contain boundary layer flows having three-dimensional large-scale (time as well as space) turbulence, secondary flow structures, coherent structures, etc. Different and complex fluid flow behaviour occurring at same time can generate such complicated structures, which may be modelled or partially resolved on time scale and length scale basis. The bed shear and velocity plays a vital role in identify the anisotropy of this complex fluid flow and its behaviour. Furthermore, the velocity distribution over gravel bed of such hydraulic resistance for turbulent flow have been extensively studied and recognised by many past investigators. Such investigation require prior knowledge of shear stress and it distribution on the channel boundary Sarma et al. (1983). The direct measurement of shear stress at various location of cross section grid of gravel bed wetted surface is extremely difficult. One of the prior based and widely acknowledged technique is Preston tube, which is based on a known velocity distribution. However, the incompetency of those methods over gravel bed was first recognised and redefined by Jin (1995) considering extra roughness parameters in the robust empirical equations, which is discussed later.

The logarithmic velocity profile equation is mostly used to predict the depth averaged velocities of wide-open channel flow with rough plane bed and free surface. Moving further, more recently researchers developed ordinary differential equation (ODE) using the Reynolds-averaged Navier-Stokes equation and log wake eddy viscosity model to predict velocity distribution accurately Rafik (2011). For the ODE obtained in their studies, they gave two semi-analytical solution i.e. the full dip-modified-log-wake law and a simple dip-modified-log-wake law. This empiricism is commonly used for closure of models obtained from force balance equations.

On the other hand, boundary shear play a vital role in estimating flow carrying capacity of a channel, sediment transportation, erosion of the river. Moreover, bed shear stress patterns results from complex flow behaviour from gravel bed also affects the anisotropy as mentioned above for velocity distribution. Prandtl's secondary currents also plays a vital role in the flow dynamics, which depends on the undulating bottom shear stress distribution in the transverse direction (Nezu et al. 1993). The theoretical acknowledgement of Prandtl (1933) and Von Karman (1921, 1930) on the flow through pipes, and the experimental studies of their associate Nikuradse (1933) not only gave rational formulae for pipe flow but also influenced the initial formulas obtained for open channel flow. Knight et al. (1984) compared the boundary shear stress in open channel flow and the closed conduit flow at comparable aspect ratio. Different distribution pattern and the mean resistance coefficients because of different secondary flow structures were observed for smooth and rigid channels. The present study is based upon a progressive lab experimentation in which a straight channel having sediment loads are under consideration. In many instances of lab research, experiments were conducted on straight channels with different geometries and depths (Banerjee et al. 2018). Ghosh and Kar (1975) reported the effect of geometry and roughness on the interaction and the variation of boundary shear distribution in the open channel flows. The distribution of boundary shear stress around the wetted perimeter in open channels is known to rely on the form of the cross section, the longitudinal variation in platform geometry, the boundary roughness distribution and the structure of secondary currents (Khatua and Patra 2007). Patra and Kar (2000), Khatua and Patra (2007) and Naik et al. (2017a) presented a method in which they presented the percentage shear stress model for the compound channel and shown

the effect of different parameters on boundary shear calculations. The significance of comprehension boundary shear stress distributions is appeared by the local or mean boundary shear stress in many hydraulic equations concerning resistance, sediment, and dispersion or cavitation problems. For estimation of the bed load transfer in open channel flows, one must divide the bottom shear stress from the total shear stress. Overall, precise calculation of the local or mean shear stress is a complex method including turbulence models. As an option, different observational, investigative or rearranged computational strategies were produced. Pretty much of them depend on splitting the channel cross section into sub-regions in which, the weight of fluid is balanced by shear force acting along the corresponding wall sections for calculation of the local, mean wall, and the mean bed shear stress in channels.

The computational approach is significantly used worldwide because of the capability and range of complexity of flow, which can be instinctively modelled and resolved according to the modeller's requirements. In this investigation, simulation-based calculation is undertaken for modelling gravel bed for estimating velocity and bed shear stress dissemination over the channel longitudinally. The results obtained through these computational approaches are therefore contrasted with the experimental data obtained for the gravel bed inbank flow.

2. Literature survey

2.1. Velocity distribution

Sarma et al. (2000) define velocity distribution law by considering velocity dip into account in open channel flows. He utilises summed up type or binary version of velocity distribution, in which for the inner section logarithmic law and for the outer section parabolic law are coupled.

Wilkerson and McGahan (2005) created two models for anticipating depth-averaged velocity distributions. The first model is used when the depth-averaged velocity data is available and the later model is used only when predicted depth-averaged velocities are within the range of 20% of actual velocities. He utilises information of past three reviews for straight trapezoidal channels having a small width due to which form drag on the fluid exerted by the bank is dominant and in this way, the depth-averaged velocity distribution is controlled. The information they utilised for working up the model are free from the impact of secondary current. The first model required measuring velocity data for calibrating the model coefficients, though the second model utilised prescribed coefficients.

Knight and Sterling (2000) analysed the lateral distributions of depth-averaged velocity and boundary shear stress by utilising the new approach of Shiono and Knight (1988) Method (SKM) for runs in straight prismatic channels that additionally accounted secondary flow effect. It justifies for bed shear, lateral shear, and secondary flow effects coefficients- τ, λ, and Γ – along these lines fusing some key 3D flow feature into lateral distribution model for stream wise motion. This technique used to examine in the straight trapezoidal open channel. Afzal et al. (2007) used power law of velocity profile to envelope the friction factor in fully developing turbulent pipe and channel flows. The model so created gives a decent estimation for low Reynolds number

in outlining procedure of a real framework contrasted with vast law.

Yang (1996) examines depth-average shear stress and velocity in rough channels. The equation is inferred for the depth-averaged shear stress in common open channels in light of a hypothetical connection between the depth-averaged shear stress and boundary shear stress. He additionally modelled an equation for depth mean velocity in a rough channel which incorporate impact of water surface (or dip phenomenon) and roughness.

Castro-Orgaz Oscar (2011) utilises the accessible data on turbulent velocity profiles in steep flow to establish the general model by considering both the laws of the wall and wake. Once the velocity profile is characterised, proportionate power-law velocity estimation is proposed, with summed up coefficients dictated by sound approach. The outcome for the turbulent velocity profiles were connected to decide the resistance characteristics for channel flows.

Albayrak and Lemmin (2011) direct examination on a wide channel having a rough non-movable bed, with a higher bed roughness and higher Reynolds number of complex secondary current dynamics within the water column and free surface of an open channel flow. He combined the results of three instruments, Acoustic Doppler Velocity Profiler (ADVP), Large-Scale Particle Image Velocimetry (LSPIV) and hot film for legitimate estimations.

Kundu and Ghoshal (2010) proposed a condition for the mean velocity dissemination of steady and uniform turbulent flow through straight open channels by consolidating the log law for an inward area and the parabolic law for the generally solid external area and checked it with the exploratory dataset. It is found that sediment concentration assumes a critical part and significantly affects the velocity dissemination for the moderately feeble external area.

2.2. Boundary shear stress distribution

Seven decades back, Leighly (1932) proposed a thought of utilising conformal mapping to express the boundary shear stress dissemination in an open-channel stream. He centered that, if the secondary flow currents are not accounted then the boundary shear stress at the bed surface must be static. Einstein's (1942) hydraulic radius separation strategy is still comprehensively utilised as a part of research facility. Einstein (1942) recognised the cross-sectional zone into two distinct regions A_b and A_w and foreseen that at the downstream segment of the liquid range A_b was static by the bed resistance. Similarly, A_w was balanced by the sidewalls resistance. The potential energy conveyed by A_b was diminished by the bed surface, and the potential energy giving by area A_w was diminished by the sidewalls. In any case, he did not propose any strategy for deciding the correct area of division line.

Knight (2007) utilise Preston-tube method and watched the dissemination of boundary shear stress in circular conduits flowing in part full smooth and rough level bed for a data going from $0.375 < \tau < 1.96$ and $6.5*10^4 < \tau < 3.42*10^5$. His study shows that the distribution of boundary shear stress depends on geometry and Froude number. The outcomes have been broke down as far as the variation of local shear stress with perimetric separation and the rate of total shear force following up on wall or bed of conduit. The consequences of %SFW have been appeared to concur well

with Knight (1981) observational equation for prismatic channels. The interdependency of secondary flow and boundary shear stress has been built up and their implications for residue transport have likewise been inspected. Yang and Mc Corquodal (2004) built up a technique by applying an order of magnitude investigation to join the Reynolds conditions in smooth rectangular channels to register the three-dimensional Reynolds shear stresses and boundary shear stress appropriation. The relationship was created as a power law with an example of n = 1, 2, or infinity.

Hardy et al. (2003) gave a technique to check the accessibility of the CFD code to an open channel flow application where the correct solution is not known: This method is based upon a Grid Convergence Index (GCI). The GCI technique for identifying the sensitivity of a model solution through numerical discretization was initially proposed by Roache (1994). The idea of GCI is mainly dependent on the geometric multigrid procedure and the sensitivity of grid, which helps to agglomerate the equation of the fine level cells to directly obtain the discretised equation for the corresponding coarser cell. The theory of grid convergence helps to associate the uncertainty with the solution at a particular resolution of grid to another finer or coarser resolution, which can help the modeler to save computational resource and time with best possible results.

Lane et al. (2004) presented a method where digital elevation data were used by close range photogrammetry and combined the data with a numerical porosity treatment of the bed to model very details of the flow incorporating the influence of the individual grains on the flow field. This gives a way superior method for roughness treatment than the method usually used such as boundary-fitted coordinates and a roughness length treatment of boundary roughness. In addition, Lane et al. (2004) suggested a modification in the CFD software packages to iteratively compute wall roughness height in individual cells based on the porosity of cells, as well as the technological capabilities to implement close-range digital photogrammetry to produce the digital elevation model (DEM).

Guo and Julien (2005) solved the continuity and momentum equations for smooth rectangular open-channel flow and proposed a technique for deciding the average bed and sidewall shear stresses. The review demonstrates that the shear stresses rely on upon different parameters like secondary flow, and interfacial shear stress. A model was developed for the instance of steady eddy viscosity with no incorporation of secondary flow. The model proposed marginally overestimated the normal bed shear stress estimations and the average sidewall shear stress was found having percentage error of 17% with respect to higher aspect ratio.

Carney et al. (2006) proposed a method to counter the coarse bed utility in the CFD packages through investigating natural channel with large bed roughness. The 'law of wall', which is certainly persist outside the laminar zone, is defined as the semi-logarithmic relationship between velocity and distance from the wall. This plays a vital role in the context of modelling since the option of standard and scalable wall function associated with the near wall treatment or wall function in model are completely based on the law of wall. These wall function account for the transition of simulation based results from the no slip condition near wall to the turbulent flow away from the wall, which gives

the dynamicity to the solution since the entire flow field is well dissected from the solid boundary to the full turbulent flow (Carney et al. 2006).

The effects of natural boundary roughness can also be integrated into the CFD modelling through drag force concepts. Nicholas (2005) developed a drag force representation of the bed roughness where drag coefficients are based on the bed topography profile. The Nicholas (2005) methodology effectively signify the effects of bed resistance, although bed topography profiles are not easily collected.

Lashkar and Fathi (2010) investigated the rectangular channels to decide the impact of wall shear force on total boundary shear force. They divided the overall results through nonlinear regression technique to decide the percentage of wall and bed shear force on the wetted perimeter for the rectangular channels.

Rameshwaran et al. (2011) contrasted the results obtained from the RANS (Reynolds Averaged Navier-Stokes) based model with the DANS (Double Averaged Navier-Stokes) based model for setups of fine gravel bed and gravel bed with large, widely spaced pebble cluster bed. The results obtained from these analyses gave a wide applicability of the RANS based model on the ground of averaged velocity and turbulent kinetic energy vertical profile. This argument justified the standard wall function modelling approach and its suitability in congruence with the RANS model. However, the overestimated prediction of turbulent kinetic energy near bed region of the pebble cluster was found due to the inability of RANS equation to completely model the higher order turbulence (length scale and time scale wise).

3. Experimental setup

A straight trapezoidal channel as a tilting flume having measurements of length 10 m, top width 0.9 m, base width 0.65 m and depth of 0.125 m was fabricated with the gravel bed (non-movable) with adjustable bed slope. The tilting flume is made of the metal frame with glass walls at the test reach. A baffle wall are fitted before the head gate for moderating high energy flow coming from overhead tank to attain a more generalised uniform flow over the channel segment. Furthermore, head gate lessens the waves and the turbulence generated due to sudden discharge of water coming from outlet of overhead tank. For measuring the bed slope, tailgate was fitted toward the end of the flume. There was an arrangement of an overhead platform in the flume, which helps in exploratory works. The flume was kept upheld on a pivot at the centre which when hydraulically operated through powered jack gave the appropriate height to the bed for maintaining the bed slope. The overall plan view and dimension of the fabricated channel is shown (Figure 1).

The entire channel is fabricated through gravel of size 13.5 mm for maintaining a no-load condition in the bed with very mild slope. The no-load condition of regime 1 is well explained by the Recking (2006) where bed load does not move with flow. No load condition resembles the case where $\sqrt{\frac{8}{f}}$ (where f is the friction factor) increases, flow resistance decreases with increasing flow depth. This category of gravel bed does not face bed load transport but as the $\frac{R}{D}$ (R is hydraulic radius and D is the diameter of gravel)
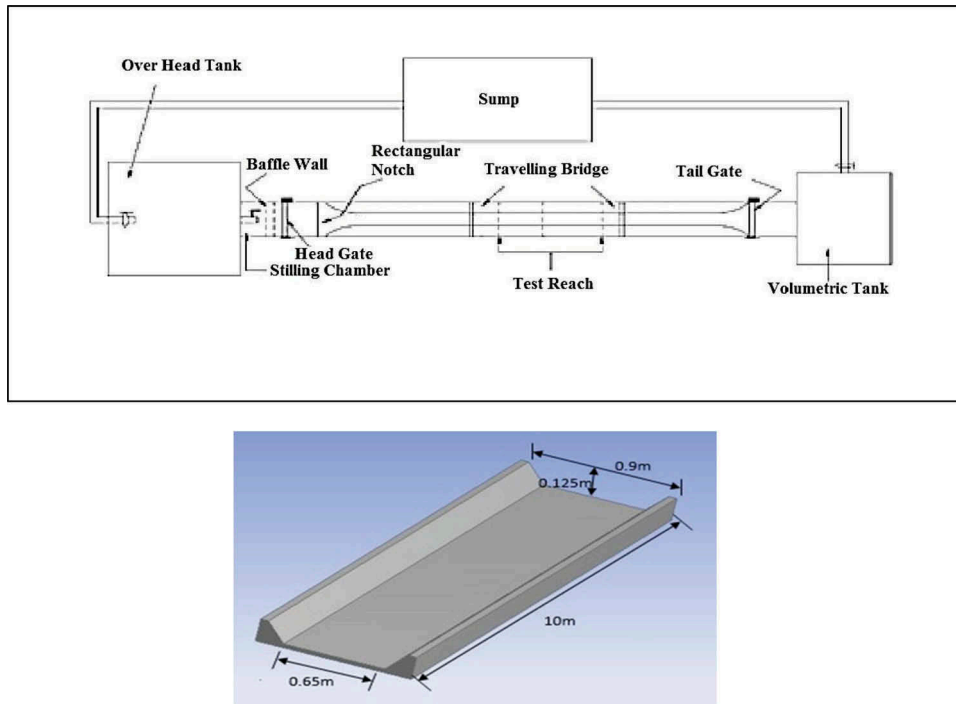
Figure 1. Plan view of the experimental channel & Overall view of the flume with experimental set up.

value increases with respect to $\sqrt{\frac{8}{f}}$ it starts sensing incipient motion and finally the bed movement comes into picture.

The roughness height was observed to be 2.5 cm. The mild slope of the flume is settled at 0.0025 (0.25%) for all runs in accordance to maintain the no-load condition. Sieve analysis was carried out for calibrating gravel of 13.5 mm grain of D_{50} size. Furthermore, the density of the sediment for 13.5 mm gravel size was found to be 1520 kg/m³.

The depth of flow in the channel was measured by using a point gauge fixed on the traveling span, which was operated manually. Point velocities are measured utilising a Micro-Pitot tube of 4.77 mm outer width with an appropriately inclined manometer at various areas over the predefined channel segment. Guide rails are given at the top point of the test flume on which a moving extension is transverse throughout the longitudinal course of the test channel. The point gauge connected toward the moving platform can be moved in both longitudinal and transverse direction. The Pitot tube is physically pivoted normal to the mainstream direction until it gives a maximum deflection of manometer reading. The water streaming out at the downstream end of the test channel was collected to a volumetric tank of area 20.866 m². The adjustment in the depth of the water with time is measured by stopwatch in a glass tube indicator with a scale having a least count of 0.01 mm.

Same micro-pitot tube of outer diameter of 4.77 mm in combination with an appropriately inclined manometer was utilised to quantify velocity. The Pitot tube is settled to the primary scale having Vernier scale with least count of 0.1 mm. The distinction in water height gives the velocity at the specific point (u) where the Pitot tube was mounted furthermore the pressure difference (Δp) by utilising the accompanying Bernoulli conditions (White Frank (1999)) is given by:

$$u = \sqrt{2g\Delta h\ sin\alpha} \qquad (1)$$

$$\Delta p = \rho g\Delta h\ sin\alpha \qquad (2)$$

Where g is the gravitational force, ρ is the density of water, Δh is the difference in water elevation in the manometer, and α is the angle of manometer with horizontal base.

While taking velocity readings utilising Pitot tube, the tube is placed confronting the direction of the flow and after that is turned along a plane parallel to the bed, until it enlists generally a maximum head difference in the connected manometer. The total head h read by the Pitot tube at the location in the channel is utilised to give the magnitude of the total velocity vector as:

$$u = \sqrt{2gh\ sin\alpha} \qquad (3)$$

At the same time, the tube coefficient is taken as a unity and the error because of turbulence in the calculation of u is neglected. In the present review, all estimations were done under uniform stream condition by managing the outflow through the downstream tailgate. Investigations were also directed under no load condition. For no load condition, total five depths out of seventeen has been taken for velocities conveyance and boundary shear stress under no load stream condition. Boundary shear stress identifies local force to the neighbourhood compelled by the liquid on a surface and thus becomes the principle reason of residue transport related to disintegration of sediments. There are a few techniques used to assess boundary shear stress in an open channel. The Preston tube strategy and energy gradient technique have been prominently utilised as a part of research facilities and in the real time field study where the channel surface was either smooth or rough (Ackermann et al. 1994; Atabey 2001; Birmingham data). In the present study of 13.5 mm gravel size bed, Preston tube technique has been utilised for flows over rough surfaces. An extra parameter for roughness has been added for situations more complicated such as rough bed (Jin 1995). A Preston tube with given external diameter d on a rough surface with characteristic roughness height k (2.5 cm) will have effective wall distance of y_c. The dynamic pressure can always be

estimated as the difference of overall pressure to the static pressure corresponding to a given effective wall distance y_c:

$$(p - p_o) = \frac{\rho}{2}\left(u^2\right)_{y=yc}; \quad y_c = k + k_c \frac{d}{2}; \frac{\Delta p \ d^2}{4\rho v^2}$$
$$= \frac{1}{2}\left(\frac{\tau_o d^2}{4\rho v^2}\right)\left(\frac{u}{u_*}\right)^2_{y=y_c} \tag{4}$$

where p is the total pressure, p_o is the static pressure, ρ is the density of fluid, u is the average velocity, k_c is a displacement factor accounting the deviation of the effective centre of the Preston tube from the geometric centre and also is a function of Reynolds number, Δp is the change in the pressure, τ_o is the boundary shear stress, v is the kinematic fluid viscosity and the u_* is the shear velocity.

Hydraulic softwares like CES works on the depth integration of the RANS conditions for the calculation of depth integrated velocity in the streamwise course. The essential type of the depth-averaged momentum equation for application on channel stream is (Shiono and Knight (1988)]):

$$\rho\left[\frac{\partial}{\partial x}(UV) + \frac{\partial}{\partial x}(UW)\right] = \rho g S_o + \frac{\delta \tau_{yx}}{\delta y} + \frac{\delta \tau_{zx}}{\delta z} \tag{5}$$

Where, x is streamwise direction parallel to the bed (m), y islateral distance across section (m), U, V, W are the velocity component in x, y, z direction respectively, S_o is the bed slope (m/m), U_d = depth-averaged streamwise velocity (m/s), V_d = depth-averaged lateral velocity (m/s), τ_{yx} = Reynolds stress (N/m^2), τ_b = bed shear stress (N/m^2). An effort has been made to investigate the velocity profiles and boundary shear stress dissemination for various depths of a straight trapezoidal channel having sedimentation as no load condition by utilising a computational fluid dynamic (CFD) modelling tool, named as ANSYS-FLUENT. The CFD model has been used to investigate the impacts of flow because of the robustness and computation ability of the packages like ANSYS to reproduce the experimental flow to par extent on the simulation based system. The computational based velocity field for every situation is contrasted and compared with lab-based estimations of velocity distribution and boundary shear stress distributions. Computational Fluid Dynamics (CFD) is a scientific approach, which is utilised to model open channel running from in-bank to over-bank streams. Diverse models are utilised to unravel Navier-Stokes conditions, which are the representing condition for any fluid flow. Finite volume method is connected to discretise the representing conditions. The exactness of computational outcomes relies on the work quality and the meshing criteria (structure or unstructured in general) used to re-enact the stream.

Unstructured mesh have cells and nodes, which are not arranged in rows and columns. Prism, pyramid and/or tetrahedron type of elements can be generated in unstructured meshes of 3D geometries. Tetrahedal mesh might use up to six times as many elements as hexahedral one, thus resulting in more computationally expensive mesh for the same number of nodes. The disadvantages of structured grid are that it is limited to simple geometries and it is time consuming to create a high quality mesh, while unstructured grid can be generated very fast for very complex geometries.

4. Result

4.1. Longitudinal velocity distribution from experimental data

Pitot tube were used to measure velocity at different longitudinal grid position along the way opposite to stream course. Velocities were measured at each *0.2 h* intervals where *h* is the stream depth (Figure 2). These deliberate estimations of velocity were utilised to plot velocity profiles and the values were utilised for contrasting and results from ANSYS FLUENT and CES.

Detailed experimentations of complete five depths have been performed and contour maps were set up over the stream segment. Figure 3 shows the contour maps for different flow depths in trapezoidal channel with gravel bed. At lower depths, least velocity happens at the bed due to no slip condition while at the free surface velocity is found to be highest. When the depth increases the strings of higher velocity happens at the free surface of the wall. However, for higher stream depth the maximum velocity does not happen amidst the free surface yet happen along the edge of the free surface. This might be because of more uniformity in high flow depths in such channels.

4.2. Application of numerical analysis

4.2.1. Velocity distribution obtained from ANSYS

In this review, a couple of simulation was accomplished by utilising the commercial code of ANSYS-FLUENT to simulate and replicate the present exploratory examination. Total five-flow depth were considered for no load conditions. A gravel bed of 13.5 mm gravel size (D$_{50}$ size
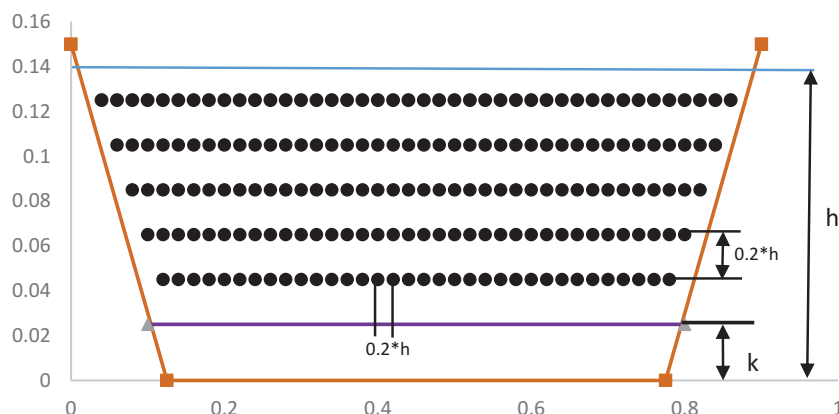
Figure 2. Typical grid showing the arrangement of velocity measurement points at the test sections.

a. Longitudinal velocity contour of flow depth 0.07 m

b. Longitudinal velocity contour of flow depth 0.08 m

c. Longitudinal velocity contour of flow depth 0.086m

d. Longitudinal velocity contour of flow depth 0.0916 m

e. Longitudinal velocity contour of flow depth 0.10m
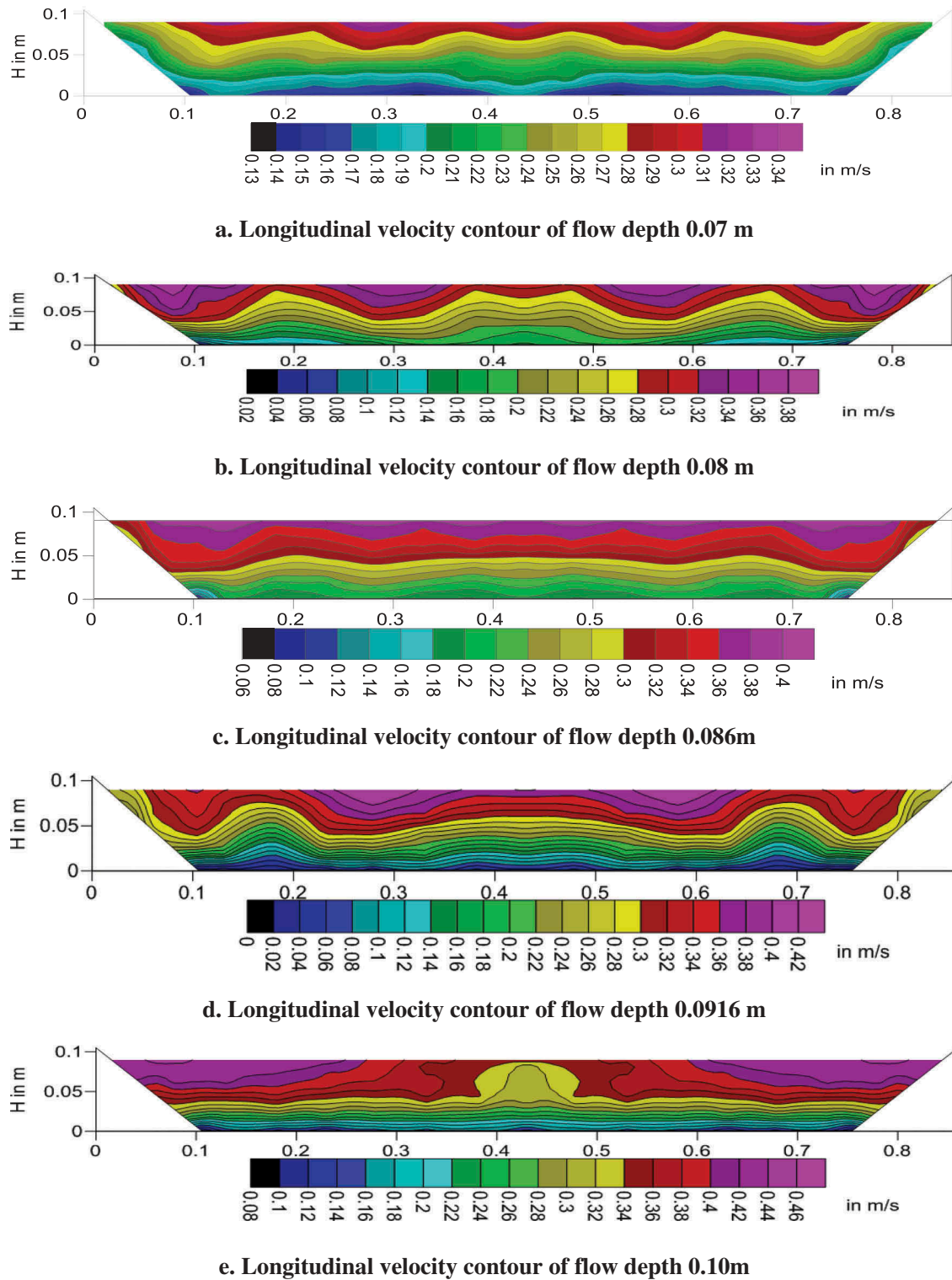
Figure 3. (a) Longitudinal velocity contour of flow depth 0.07 m. (b) Longitudinal velocity contour of flow depth 0.08 m. (c) Longitudinal velocity contour of flow depth 0.086m. (d) Longitudinal velocity contour of flow depth 0.0916 m. (e) Longitudinal velocity contour of flow depth 0.10m.

Table 1. Values of the constants in the k-ε model for open-channel flows.

C_μ	$C_{\varepsilon 1}$	$C_{\varepsilon 2}$	σ_k	σ_ε
0.09	1.44	1.92	1.2	1.2

categorised through sieve analysis) was utilised as a part of beds for inbank flow to foresee the velocity dispersion along the channel bed. Here the k-ε model is utilised as a turbulence closure model. The k-ε conditions are discretised in both space and time. The K-ε is most famous two-equation turbulence closure method, which is found in many CFD commercial codes viz. ANSYS. Even in steady flow, small high-frequency fluctuation can be seen and to account for these, time averaging methodology is used, which in turns gives additional terms, which need empiricism (mostly for the transport equation of kinetic energy and dissipation/frequency terms). These additional terms need to be expressed as calculable quantities for closure solutions. It

is a semi-empirical model based on model transport equations for the turbulent-kinetic energy 'k' and its dissipation rate 'ε', and is expressed by the following equations:

$$\underbrace{\frac{\partial k}{\partial t}}_{\substack{Rate\ of\\ change\\ of\ k}} + \underbrace{U_i \frac{\partial k}{\partial x_i}}_{\substack{Convenctive\\ transport\\ of\ k}} = \underbrace{-\frac{\partial k}{\partial x_i}\left[\overline{u_i'\left(\frac{u_j' u_j'}{2}+\frac{p'}{\rho}\right)}\right]}_{Turbulent\ transport\ of\ k} \underbrace{-\overline{u_i' u_j'}\frac{\partial U}{\partial X_j}}_{\substack{P=turbulence\\ production}}$$

$$\underbrace{-\nu\overline{\frac{\partial u_i'}{\partial x_i}\frac{\partial u_i'}{\partial x_i}}}_{\substack{E=rate\ of\\ dissipation\\ of\ k}}$$

(6)

The exact k-equation is of no use in the turbulence model since new unknown correlations appear in the turbulent transport and dissipation terms. To obtain a closed set of equations, model assumptions must be introduced for these terms. Assuming that the turbulent transport of k is proportional to the gradient of k (Rodi 1993):

$$\overline{u_i'\left(\frac{u_j' u_j'}{2}+\frac{p'}{\rho}\right)} = \frac{\nu_t}{\sigma_k}\frac{\partial k}{\partial x_i}$$

(7)

where σ_k is the turbulent Schmidt number that does not have a universal value and empirical values have been used in different studies in the range of 0.2 – 1.3 (Tominaga and Stathopoulos 2007). The selected value of σ_k has a significant effect on the prediction of the results. Thus, Tominaga and Stathopoulos (2007) recommended that σ_k should be determined by considering the dominant flow structures for each case. However, σ_k generally takes value around 1.0 (*e.g.* Nezu et al. 1993, Pope 2000, Rodi 1993).

Furthermore, Reynolds stress tensor can be related to mean flow field through:

$$-\overline{u_i' u_j'} = \nu_t\left[\frac{\partial U_i}{\partial x_i}+\frac{\partial U_i}{\partial x_i}\right] - \frac{2}{3}k\delta_{ij}$$

(8)

where ν_t is the eddy viscosity, δ_{ij} is the kronecker delta ($\delta_{ij}=$ 1 for i = j; and $\delta_{ij}=$ 0 for i≠j); and k is the turbulent kinetic energy, defined as $k = \overset{i\ i}{uu}/2$.

Using above equations 7 and 8 one can write:

$$\underbrace{\frac{\partial \varepsilon}{\partial t}}_{\substack{Rate\ of\\ change\ of\\ \varepsilon}} + \underbrace{U_i\frac{\partial \varepsilon}{\partial x_i}}_{\substack{Rate\ of\\ change\ of\\ \varepsilon}} = \underbrace{\frac{\varepsilon}{k}(C_{\varepsilon 1}P - C_{\varepsilon 2}\varepsilon)}_{\substack{Production\ and\\ dissipation\ rate\\ of\ \varepsilon}} + \underbrace{\frac{\partial}{\partial x_i}\left(\frac{\nu_t}{\sigma_t}\frac{\partial k}{\partial x_i}\right)}_{\substack{Turbulent\\ transport\ of\ \varepsilon}}$$

(9)

where the eddy viscosity used in the model is specified as

$$\nu_t = C_\mu k^2/\epsilon$$

The k-ε method uses five empirical constants, which are given in table below. Their standard value for open channel flow are based on the capability of the model to the logarithmic velocity distribution near the wall in channel flow with Von-Karman constant k = 0.4 (Nezu et al. 1993) shown in Table 1.

In the present work, the coupling amongst pressure and velocity field is considered using PISO technique, which is the pressure implicit splitting operator used in Fluent (Issa (1986)).

(Figure 4(a–e)) shows the velocity distribution simulated in ANSYS for no load conditions. In this present scenario, it has found that ANSYS results were well matching with the data collected from the experiment. The overall distribution shown in these results are not as dynamic as that of the contours presented in the Figure 3. However the maximum velocity obtained and also the distribution of velocity is almost equivalent to the experimental reults obtained.

4.2.2. *Comparison of boundary shear stress distribution*

Boundary shear stresses were measured from an indicating point along the wetted perimeter of the channel by utilising Preston tube of diameter 4.77 mm alongside the different longitudinal separations. A total five stream depths considered throughout the experimental procedure were kept same here for boundary shear stress distribution. The measured point boundary shear stresses (τ) are plotted across the flow domain for no load flow condition in (Figure 4 (a–e)). From this figure, it can be presumed that for both exploratory and numerical outcomes, most boundary shear stress happens at the interface between channel bed and the sidewall of the trapezoidal channel. Boundary shear at both ends is observed to be same for all flow depths, nonetheless, at the centre of the channel, the trend increases for the boundary shear stress with increment in flow depths. All the numerical programming found to give great outcomes when contrasted with exploratory outcomes. Nevertheless, ANSYS found to give more precise when contrasted with CES.

CES is a semi-programming, which produces the 1D result for all flow condition. It is based on depth-averaged of RANS equation as mentioned beforehand for any type of flow characterisics. For both these software initial and boundary condition and roughness value has as same as the experimental data. Roughness value for the bed, right bank and left bank is shown in Table 2 which is taken as the roughness input in CES while in ANSYS fluent the boundary condition are given in the Table 3. For a calculation domain with water and air the VOF (volume of fluid) method is used to calculate the free surface. The free surface modelling of VOF is well used for tracking and locating the free surface. The numerical method of VOF is based on Eulerian approach whose algorithm works on the principle of scalar fraction function.

(Figure 5.(a–e)) demonstrates the plot obtained for boundary shear stress distribution between experimental data with CES and ANSYS. From these figures, we observed that CES over anticipate the boundary shear though ANSYS underestimates the experimental data. Therefore we can generalise that ANSYS gave a superior results in contrast to CES, though ANSYS underestimates but follows overall trend especially near the side slope. Side slope have more tricky dissemination due to secondary circulation which changes its direction near the interface.

On the other hand, (Figure 6.(a–e)) demonstrates the dissemination of depth average velocity for all data obtained. From the following figures, we can understand both CES and ANSYS underestimates the experimental data. However, we can observe from the dataset that ANSYS gives superior results than CES which can be explained on the basis of overall modeling techniques used in these two software packages. In ANSYS, a 3D model is used for simulation using K-epsilon method which itself is a turbulence closure model. The overall approach to model turbulence through transport equation and epiricism is what achieved in this model. Although, CES does
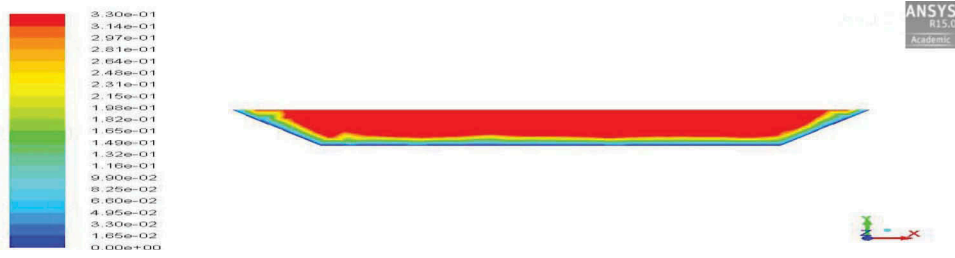
a. longitudinal velocity contour of flow depth 0.07 m using ANSYS
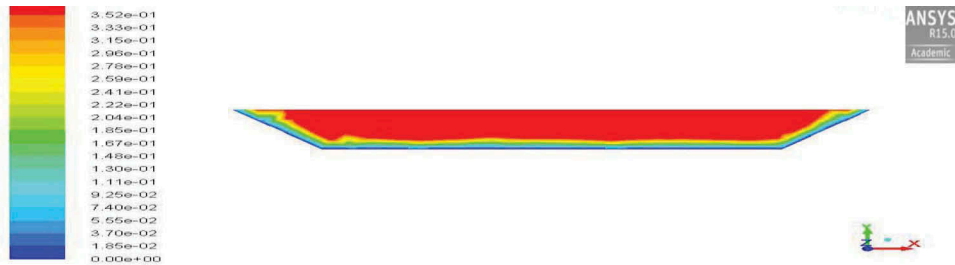
b. longitudinal velocity contour of flow depth 0.08 m using ANSYS
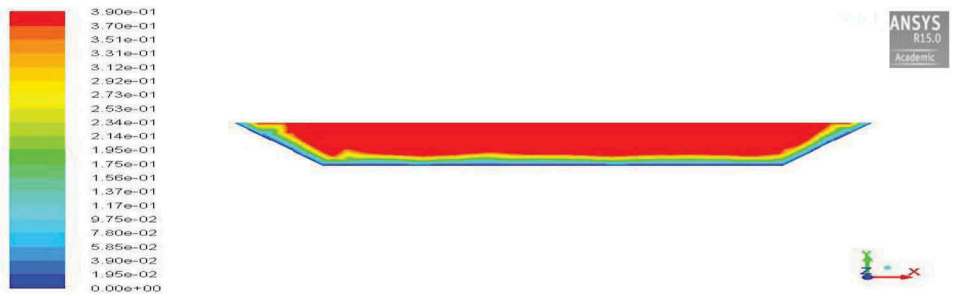
c. longitudinal velocity contour of flow depth 0.086 m using ANSYS
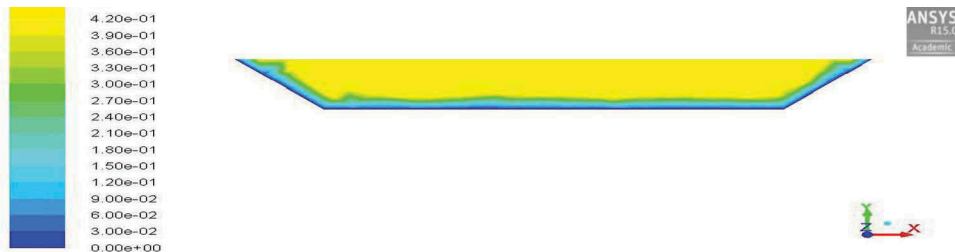
d. longitudinal velocity contour of flow depth 0.0916 m using ANSYS
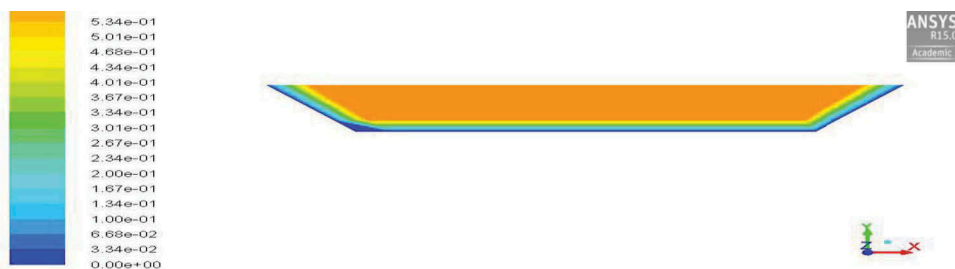
e. longitudinal velocity contour of flow depth 0.010 m using ANSYS

Figure 4. (a) longitudinal velocity contour of flow depth 0.07 m using ANSYS. (b) longitudinal velocity contour of flow depth 0.08 m using ANSYS. (c) longitudinal velocity contour of flow depth 0.086 m using ANSYS. (d) longitudinal velocity contour of flow depth 0.0916 m using ANSYS. (e) longitudinal velocity contour of flow depth 0.010 m using ANSYS.

simulation on the basis of RANS eqution for 1D modelling but does not consider the overall physic of flow. Which is quite visible in both BSS and DAV distribution graph since CES is unable to replicate the trend near bed and interface. ANSYS though produces better results but still have shortcoming which can be explained as the inability of the modeller to

Table 2. Roughness input in CES.

Roughness Zone	Material	Unit roughness	Lower – upper limit
Bed	Gravel 7–20 mm	0.025	0.02–0.028
Right wall	Concrete	0.02	0.018–0.022
Left Wall	Concrete	0.02	0.018–0.022

produce a model having full convergence, stability and consistency during simulation for dispersive as well as dissipative errors. The idea of doing both simulation was not only to check the results on the basis of DAV and BSS but was also

Table 3. Boundary conditions in ANSYS FLUENT.

Depth of flow (cm)	Inlet Constant velocity (m/s)	Bottom		Wall	
		Roughness height (m)	Wall motion	Roughness height (m)	Wall motion
10	0.6	0.025	No slip condition	0.025	No slip condition
9.16	0.41	0.025	No slip condition	0.025	No slip condition
8.6	0.39	0.025	No slip condition	0.025	No slip condition
8	0.37	0.025	No slip condition	0.025	No slip condition
7	0.33	0.025	No slip condition	0.025	No slip condition
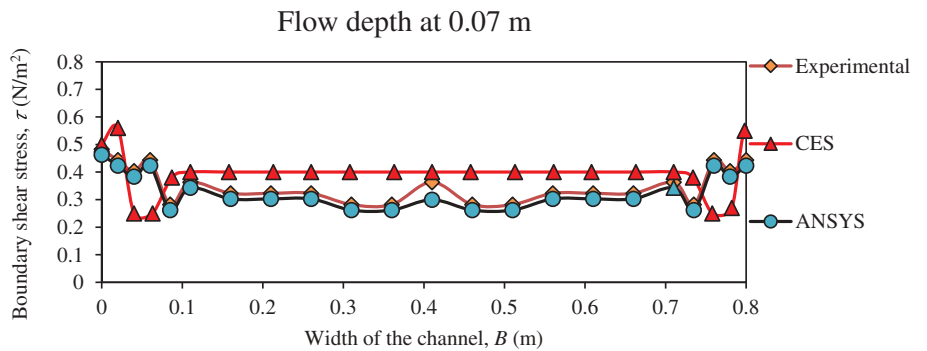
a. Comparison of Boundary shear stress distribution for flow depth 0.07m
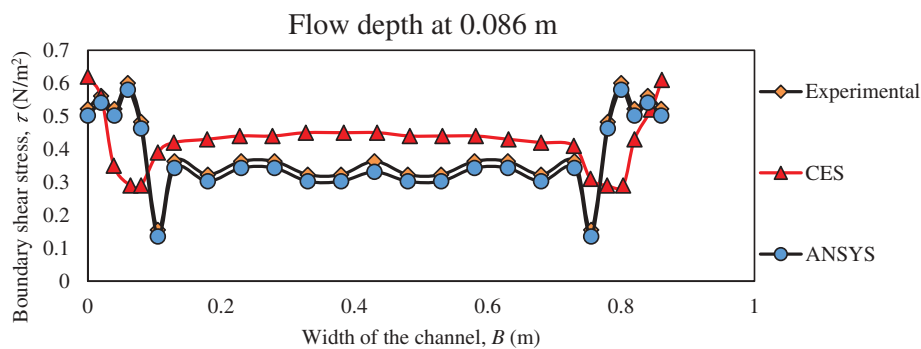
b. Comparison of Boundary shear stress distribution for flow depth 0.08m
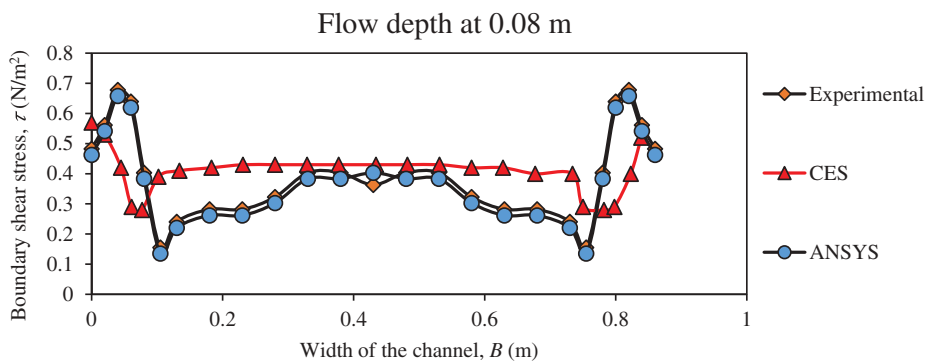
c. Comparison of Boundary shear stress distribution for flow depth 0.086m

Figure 5. (a) Comparison of Boundary shear stress distribution for flow depth 0.07m. (b) Comparison of Boundary shear stress distribution for flow depth 0.08m. (c) Comparison of Boundary shear stress distribution for flow depth 0.086m. (d) Comparison of Boundary shear stress distribution for flow depth 0.096m. (e) Comparison of Boundary shear stress distribution for flow depth 0.10 m.

Flow depth at 0.0916 m

d. Comparison of Boundary shear stress distribution for flow depth 0.096m

Flow depth at 0.10 m
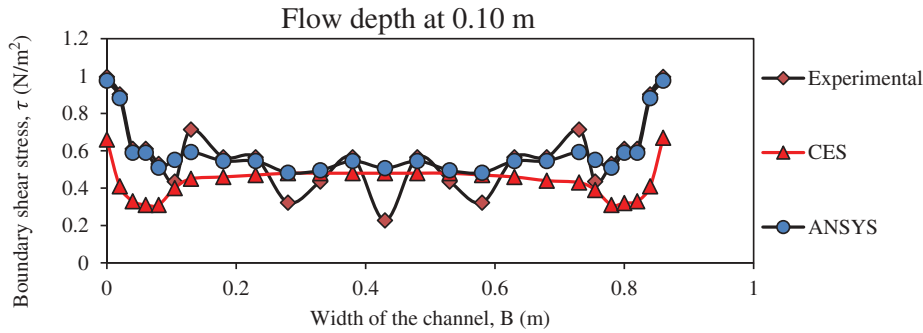
e. Comparison of Boundary shear stress distribution for flow depth 0.10 m

Figure 5. continued.

to identify the requirements for comutational time and resources. The meshing plays important role in ANSYS even though grid convergence index is not checked here but its significance prolifertes while simulating complex flow behaviour. The results can be refined through proper analysis of meshing and triangulated irregular network generation. This could be another area of research to identify the best grid convergence on the basis of present inbank gravel bed flow condition.

Error analysis for both sets of results are done on the basis of percentage error and based on plot obtained through observed and simulated results.

5. Error analysis

To contrast the strength of the numerical model with the experimental data, a plot between observed and simulated data are obtained and shown in Figure 7. In the plots, it is clearly visible that the results obtained in depth average velocity give better results in comparison to that of boundary shear stress. The deviation of results from the line of good agreements are more viable in CES since overall physics of flow involved in its solution of the RANS model is incomplete and compromised.

Furthermore, Root Mean Squared Error (RMSE) and Nash-Sutcliffe efficiency (E) are estimated for all the depths attained for the inbank flow with no load condition.

The results obtained from these residual and efficiency estimator methods have been represented as bar charts in Figures 8 and 9.

Root Mean Squared Error or Root Mean Squared Deviation is a measure of the differences between values predicted by model or an estimator and the actually observed values. These individual differences are called as residuals when the calculations are performed over the data sample that is used for estimation, and are known as estimation errors when computed out of the sample (Naik et al. 2017b). The RMSE is defined as,

$$RMSE = \frac{1}{n}\sum_i^n (P_i - O_i)^2 \qquad (10)$$

where n is the number observation, i denotes the ith term of the series, P_i is the simulated value and O_i is the observed value.

In the Figure 8, one can see that the deviation of simulated results obtained in ANSYS is in least with the experimental results . However, its dependibility decreases as the depth of flow increases. This can be argued on the basis of complexity of flow which increases with the flow depth over side slope. This had reasonably affected the results obtained for the boundary shear stress and depth average velocity.

Nash-Sutcliffe efficiency (E) are estimated to provide more information on the systematic and dynamic errors present in the model simulation. The efficiency E proposed by Nash and Sutcliffe (1970) is defined as:

$$E = 1 - \frac{\sum_i^n (O_i - P_i)^2}{\sum_i^i (O_i - \bar{O})^2} \qquad (11)$$

where $\bar{O}$ is the mean of the observed data. The range of E lies between 1.0 (perfect fit) and $-\infty$.

The Figure 9, obtained from the Nash-Sutcliffe efficiency (E) shows the overall applicability of the numerical simulation to replicate the results obtained from the experimentation. Overall, more than 95% of NSE is visible for the ANSYS and 80%-95% for CES, which suggest that the results are in good
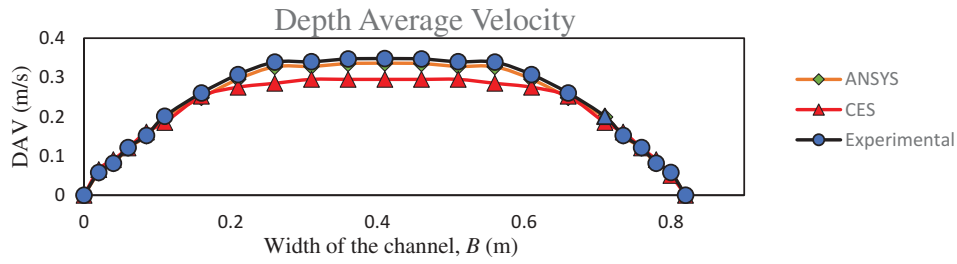
a. Comparison of Boundary shear stress distribution for flow depth 0.07 m
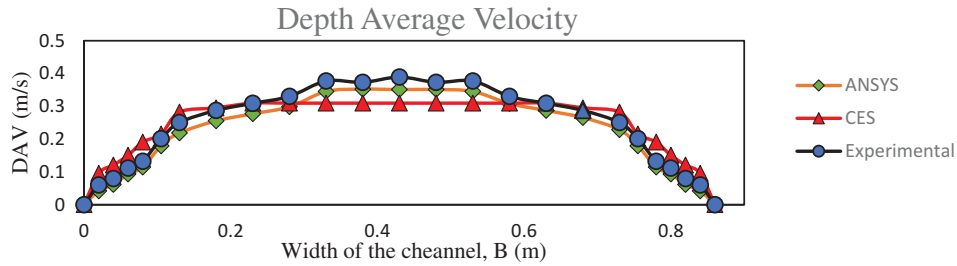
b. Comparison of Boundary shear stress distribution for flow depth 0.08 m
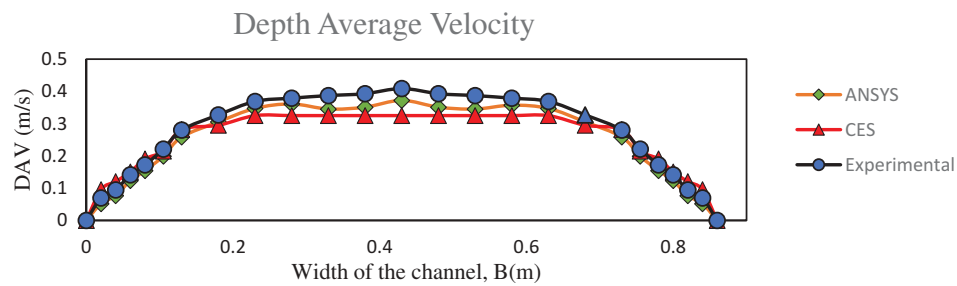
c. Comparison of Boundary shear stress distribution for flow depth 0.086 m
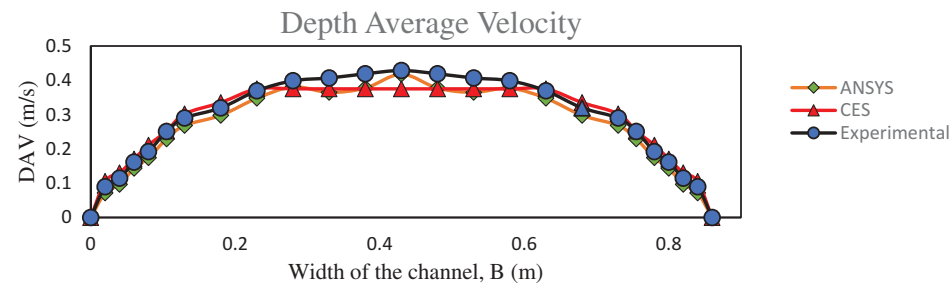
d. Comparison of Boundary shear stress distribution for flow depth 0.0916 m
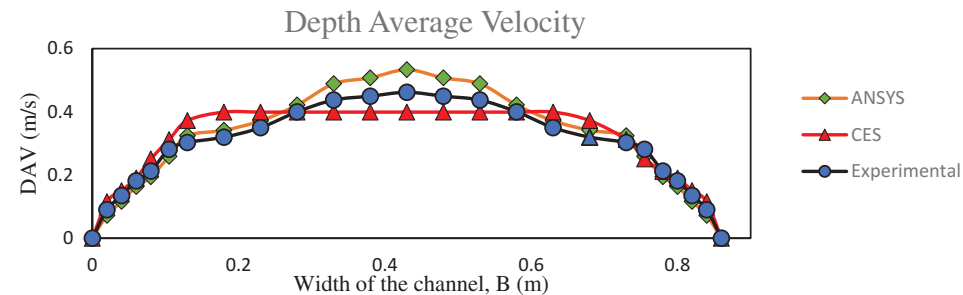
e. Comparison of Boundary shear stress distribution for flow depth 0.1m

Figure 6. (a) Comparison of Boundary shear stress distribution for flow depth 0.07 m. (b) Comparison of Boundary shear stress distribution for flow depth 0.08 m. (c) Comparison of Boundary shear stress distribution for flow depth 0.086 m. (d) Comparison of Boundary shear stress distribution for flow depth 0.0916 m. (e) Comparison of Boundary shear stress distribution for flow depth 0.1m.

agreement with the experimental analysis. However the results obtained for the higher flow depth are having least NSE which once again verify the arguments made for the higher depth flow analysis.
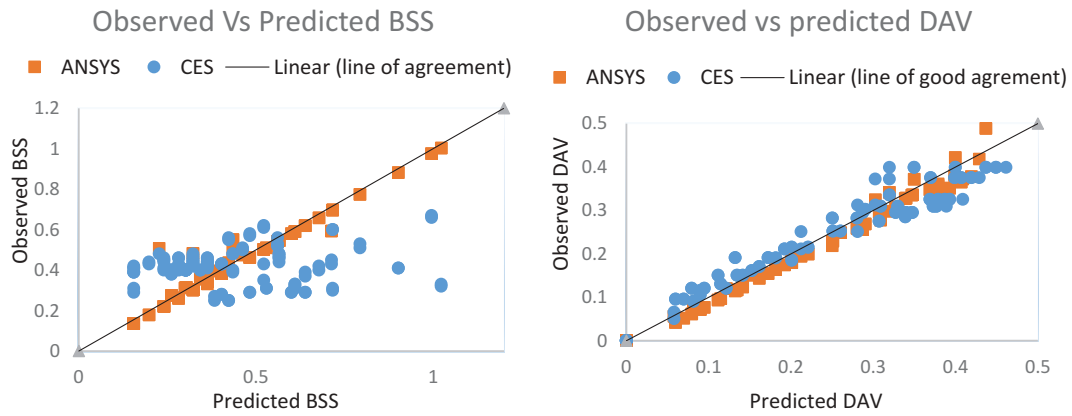
Figure 7. Observed vs simulated results obtained from ANSYS and CES for BSS and DAV.

	RMSE 0.07cm	RMSE 0.08cm	RMSE 0.086cm	RMSE 0.0916cm	RMSE 0.1cm
■ CES	0.013337445	0.026719796	0.02076744	0.090796894	0.058396982
■ ANSYS	0.000144	0.000448	0.000424527	0.0004	0.007956895

	RMSE 0.07cm	RMSE 0.08cm	RMSE 0.086cm	RMSE 0.0916cm	RMSE 0.1cm
■ CES	0.000916039	0.001710985	0.001563373	0.000504061	0.001439614
■ ANSYS	6.80017E-05	0.00055451	0.000621454	0.000571847	0.000983765
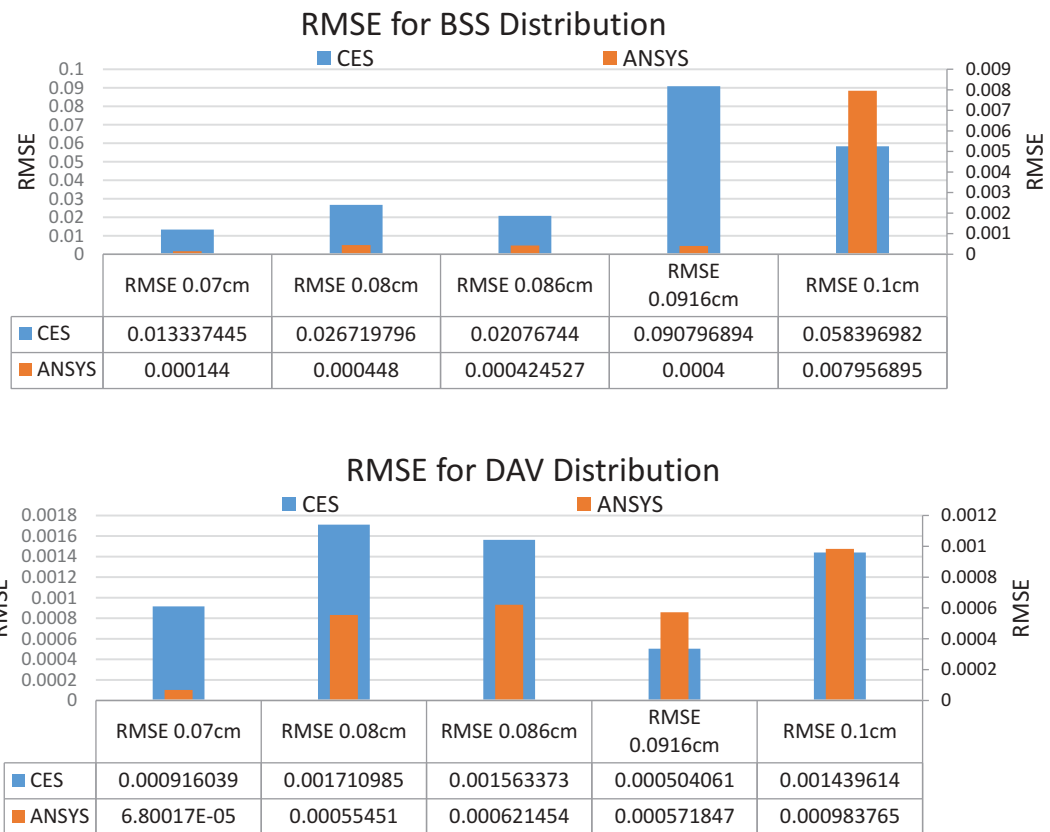
Figure 8. Root Mean Squared Error for predicted boundary shear stress and depth average velocity for five depths.

6. Conclusions

In this study, numerical analysis for prediction of depth-averaged velocity and boundary shear stress distribution for inbank flow over gravel bed with no load condition is presented. In the first part of this investigation, a 3D model of turbulence stream pattern over gravel bed were simulated using a numerical model called K-ε closure model. Using experimental and numerical analysis, variation of velocity components for inbank flow with no load condition were represented through contour mapping of cross-sectional velocity. The other part of this investigation dealt with the prediction of the depth-averaged velocity and boundary shear distribution using two different models, which are finally contrasted with the experimental data. The results of CES and ANSYS numerical model were compared and error analysis was performed to demonstrate the difference in

results obtained from these two models. The main conclusions of this study are as follows:

- The contours shown by the experimental results and ANSYS modeling are quite comparable over the range of velocity obtained throughout the mapping. The maximum velocity over the top surface in both the contour mapping is quite same, which shows that the velocity mapping is showing analogous results with ANSYS modeling. However, the dynamicity of results are very much questionable since the differential layer of velocity over the depth is not distinguishable in ANSYS modeling which is completely modeling related issue rather than the numerical model limitations.
- The local velocity towards the top surface is observed to increase with increment in the depth of flow considering no load conditions (Figure 3(d–e)). The same trends are found in the hydrodynamic modeling,

NSE for BSS Distribution

	NSE 0.07cm	NSE 0.08cm	NSE 0.086cm	NSE 0.0916cm	NSE 0.1cm
ANSYS	0.964107776	0.980509989	0.971292807	0.994966436	0.787906774
CES	0.85415	0.914725	0.863154	0.962789	0.70254

NSE for DAV Distribution

	NSE 0.07cm	NSE 0.08cm	NSE 0.086cm	NSE 0.0916cm	NSE 0.1cm
ANSYS	0.994687852	0.965559219	0.965727372	0.968800947	0.94875992
CES	0.928441012	0.893730275	0.91378146	0.972499268	0.925016712

Figure 9. Nash-Sutcliffe error for predicted boundary shear stress and depth average velocity for five depths.

which gives synonymous outcomes as for the test perceptions.

- The dip in velocity over the top surface is visible in experimental results but in ANSYS again the modeling shortcoming are visible which is quite reasonable since the computation resource available are not viable to reproduce such fine results with low quality meshing to save computation time (Figure 4).
- Furthermore, at the point when sidewall effect is available, a solid lateral velocity component (w) is coordinated close to the free surface of the sidewall to the channel centre and a down flow (v) happens from the free surface. These secondary flow components create a solid free surface vortex and the event of the maximum velocity underneath the free surface. This is noticeable in high flow depth.
- CES demonstrates uniform conveyance of boundary shear stress over the bed of the channel, while the 3D model of ANSYS-FLUENT shows comparable patterns concerning experimental insights. Boundary shear stress results obtained from CES over predicts the observations all through the horizontal cross segment for all the flow depth, with a comparative pattern. This could be explained through the concept of secondary flow generation over side slope of wide trapezoidal channel and rectangular channel. In a simpler model like CES, these complex behaviors of flow are neglected because of which the overestimation and unruly trend over the side slope are explicable.
- The depth average velocity and boundary shear stress distribution obtained from both the modeling gives similar overall trend. This shows that for the initial calculation of depth average velocity and boundary shear

distribution over gravel bed can be done over these models. However, to obtain finer results in any model it is quite clear that the 3D complex behaviour of the flow has be modeled with reasonable dependency.

- The error analysis shows that the RMSE obtained for ANYSS is very small but for CES it is quite high. It is also visible that for the higher flow depths the RMSE obtained for the ANSYS as well as CES is comparable in both boundary shear and depth average velocity distribution. NSE obtained for the ANSYS is very high in the range of 90's in both the dissemination. This again shows the promising results obtained through simulation and numerical modeling. Field engineers can use these modeling to reproduce results for any fluvial flow keeping in mind the complexity and range of modeling required for the 3D flow behaviour.

The overall idea of using numerical modelling to reproduce the inbank gravel bed flow has been carried out which shows agreeable results for this channel facility. However, secondary cell pattern, detailed velocity measurements in the water column and on the free surface are not well recognised in the distribution due to undermined physics of flow over experimental and numerical analysis. Furthermore, same experimental results if obtained with 3D equipment then the complex flow like secondary current circulation could have been easily obtained and results that are more realistic could have been investigated over side slope. This could be the future scope of the present study where no load condition can be simulated over inbank as well as

overbank flow with 3D studies including secondary circulations, coherent structures and mass transfer induced horizontal vorticity over floodplain can be investigated.

Notations

ν_t	Eddy viscosity
τ_0	Boundary shear stress
{UVW}	Velocity component in {xyz} directions
Δp	Change in the pressure (static and dynamic)
$A_b \, A_w$	Cross sectional zone
D	Diameter of the gravel
d	Diameter of the Preston tube
D_{50}	50% grain size diameter at
g	Acceleration due to gravity
h	*Flow* depth measured from bed
k	Turbulent kinetic energy
k_c	is a displacement factor accounting the deviation of the effective centre of the Preston tube from the geometric centre and also is a function of Reynolds number
p	total pressure
p_o	static pressure
Q	Channel discharge
S_o	Channel bed slope
u	Measured velocity by the manometer
$u^\star$	Shear velocity
v	Lateral velocity component
w	Vertical velocity component
x	Longitudinal/streamwise coordinates
y	Lateral/spanwise coordinates
z	Coordinate normal/vertical to bed
z	Distance between the free surface with arbitrary datum
z_0	Fraction of the bed roughness
ν	Kinematic viscosity of water
ρ	Density of water
τ_c	Critical Boundary shear stress of the channel

Disclosure statement

No potential conflict of interest was reported by the authors.

ORCID

Prateek Kumar Singh (iD) http://orcid.org/0000-0002-7439-4685
Khisanjit Kumar Khatua (iD) http://orcid.org/0000-0002-8843-211X

References

Ackermann, N.L., Shen, H.T., and Sanders, B. (1994). "Experimental studies of sediment enrichment of arctic ice covers due to wave action and frazil entrainment". *J. Geophys. Res: Oceans.*, 99(C4), 7761–7770. doi:10.1029/93JC03581

Afzal, N., Seena, A., and Bushra, A. (2007). "Power law velocity profile in fully developed turbulent pipe and channel flows". *J. Hydr. Engrg.*, 133(9), 1080–1086. doi:10.1061/(ASCE)0733-9429(2007)133:9(1080)

Albayrak, I., and Lemmin, U. (2011). "Secondary currents and corresponding surface velocity patterns in a turbulent open-channel flow over a rough bed". *J. Hydr. Engrg.*, 137(11), 1318–1334. doi:10.1061/(ASCE)HY.1943-7900.0000438

Atabey, S. (2001) "Sediment transport in two-stage channels", Ph.D. Thesis, The University of Birmingham, U.K.

Banerjee, S., Naik, B., Singh, P., and Khatua, K.K. (2018). "Flow resistance in gravel bed open channel flows case: Intense transport condition". *ISH J. Hydraulic Eng.*, 1–12. doi:10.1080/09715010.2017.1422189

Carney, S.K., Brian, P.B., and Gessler, D. (2006). "Representing the bed roughness of coarse-grained streams in computational fluid dynamics". *Earth Surface Processes and Landforms*, 31(6), 736–749. doi:10.1002/esp.1274

Castro-Orgaz Oscar, D.S. (2011). "Power-law velocity profile in turbulent boundary layers: An integral Reynolds-number dependent solution". *Acta. Geophysica.*, 59(5), 993–1012. doi:10.2478/s11600-011-0025-1

Einstein, H.A. (1942). "Formulas for the transportation of bed-load". *Trans. Am. Soc. Civ. Eng*, 107, 561–597.

Ghosh, S.N., and Kar, S.K. (1975, December). "River flood plain interaction and distribution of boundary shear in a meander channel with flood plain". *Proc., Instn. Civ. Engrs., London*, 59(Part 2), 805–811.

Guo, J., and Julien, P.Y. (2005). "Boundary shear stress in smooth rectangular open channels". *Proc., 13th Int. Association Hydraulic Research*, APD Congress, Singapore, 1, 76–86.

Hardy, R.J., Lane, S.N., Ferguson, R.I., and Parsons, D.R. (2003). "Assessing the credibility of a series of computational fluid dynamic simulations of open channel flow". *Hydrol. Process.*, 17(8), 1539–1560. doi:10.1002/(ISSN)1099-1085

Issa, R.I. (1986). "Solution of the implicitly discretized fluid flow equations by operator-splitting". *J. Comput. Phys.*, 62, 40–65. doi:10.1016/0021-9991(86)90099-9

Jin, M. (1995). "Boundary shear stress measurements by two tubes". *J. Hydraulic Res.*, 33(3), 385–395. doi:10.1080/00221689509498579

Khatua, K.K., and Patra, K.C. (2007). "Boundary shear stress distribution in compound open channel flow". *ISH J. Hydraulic Eng.*, 13(3), 39–54. doi:10.1080/09715010.2007.10514882

Knight, D.W. (1981). "Boundary shear in smooth and rough channels". *J. Hydraul. Div., Am. Soc. Civ. Eng.*, 107(7), 839–851.

Knight, D.W. (2007). "Modelling depth-averaged velocity and boundary shear in trapezoidal channels with secondary flows". *J. Hydr. Engrg.*, 133(1), 1–3947. doi:10.1061/(ASCE)0733-9429(2007)133:1(39)

Knight, D.W., Demetriou, J.D., and Hamed, M.E. (1984). "Boundary shear in smooth rectangular channels". *J. Hydr. Engrg*, 110(4), 405–422. doi:10.1061/(ASCE)0733-9429(1984)110:4(405)

Knight, D.W., and Sterling, M. (2000). "Boundary shear in circular pipes running partially full". *J. Hyd. Engg., ASCE*, 126(4), 265-275. doi: 10.1061/(ASCE)0733-9429(2000)126:4(263)

Kundu, S., and Ghoshal, K. (2010). "Velocity distribution in open channels: combination of log-law and parabolic-law". *World Acad. Science, Eng. Technol.*, 68, 2012.

Lane, S.N., Hardy, R.J., Elliott, L., and Ingham, D.B. (2004). "Numerical modeling of flow processes over gravelly surfaces using structured grids and a numerical porosity treatment". *Water. Resour. Res.*, 40, 1. doi:10.1029/2002WR001934

Lashkar, A.B., and Fathi, M.M. (2010). "Wall and bed shear forces in open channels". *Res. J. Phys.*, 4(1), 1–10. doi:10.3923/rjp.2010.1.10

Leighly, J.B. (1932). ""Toward a theory of the morphologic significance of turbulence in the flow of water in streams", Univ.". *Calif. Publ. Geography*, 6(1), 1–22.

Naik, B., Khatua, K.K., Padhi, E., and Singh, P. (2017a). "Loss of energy in the converging compound open channels". *Arabian J. Sci. Eng.*, 1–9, 2191-4281.doi: 10.1007/s13369-017-2963-7

Naik, B., Khatua, K.K., Wright, N., Sleigh, A., and Singh, P. (2017b). "Numerical modeling of converging compound channel flow". *ISH J. Hydraulic Eng.*, 1–13. doi:10.1080/09715010.2017.1369180

Nash, J.E., and Sutcliffe, J.V. (1970). "River flow forecasting through conceptual models, Part I. A discussion of principles". *J. Hydrol.*, 10, 282–290. doi:10.1016/0022-1694(70)90255-6

Nezu, I., Tominaga, A., and Nakagawa, H. (1993). "Field measurements of secondary currents in straight rivers". *J. Hydraul. Eng.*, 119(5), 598–614. doi:10.1061/(ASCE)0733-9429(1993)119:5(598)

Nicholas, A.P. (2005). "*Roughness parameterization in CFD modelling of gravel-bed rivers*". Vol. 540, John Wiley and Sons, Chichester.

Nikuradse, J. (1933). "*Laws of turbulent flow in rough pipes*". translation by National Advisory Committee for Aeronautics, TM 1292, Nov., 1950 (originally published in German in 1933)

Patra, K.C., and Kar, S.K. (2000). "Flow interaction of meandering river with floodplains". *J. Hydraulic Eng.*, 126(8), 593–604. doi:10.1061/(ASCE)0733-9429(2000)126:8(593)

Pope, S. B. (2000). "Turbulent flows". Cambridge University Press, Cambridge, United Kingdom. ISBN 0–521–59886–9.

Prandtl, L. (1933). "*Recent results of turbulent research*".

Rafik, A. (2011). "An ordinary differential equation for velocity distribution and dip-phenomenon in open channel flows". *J. Hydraulic Res.*, 49(1), 82–89. doi:10.1080/00221686.2010.535700

Rameshwaran, P., Pamela, S.N., and Lawless, M. (2011). "Flow modelling in Gravel-bed Rivers: Rethinking the bottom boundary condition". *Earth Surface Processes and Landforms*, 36(10), 1350–1366. doi:10.1002/esp.2158

Recking, A. (2006). "An experimental study of grain sorting effects on bedload." Ph.D. thesis, French engineering university INSA Lyon.

Roache, P.J. (1994). "Perspective: A method for uniform reporting of grid refinement studies". *Trans. American Soc. Mech. Eng. J. Fluids. Eng.*, 116, 405–505.

Rodi, W. (1993). "Turbulence Models and Their Application in Hydraulics: A State-of-the-Art Review". 3rd Edition, Int. Association for Hydraulic Research, Delft, Balkema.

Sarma, K.V.N., Lakshminarayana, P., and Rao, N.S.L. (1983). "Velocity distribution in smooth rectangular open channels". *J. Hydraulic Eng.*, 109(2), 270–289. doi:10.1061/(ASCE)0733-9429(1983)109:2(270)

Sarma, N.V.K., Prasad, R.V.B., and Sarma, K.A. (2000). "Detailed study of binary law for open channel". *J. Hydr. Engrg.*, 126(3), 210–214. doi:10.1061/(ASCE)0733-9429(2000)126:3(210)

Shiono, K., and Knight, D.W. (1988) "Refined modelling and turbulence measurements". *Proceedings of 3rd International Symposium, IAHR, Tokyo, Japan*, July, 26–28. doi:10.3168/jds.S0022-0302(88)79586-7

Tominaga, Y., and Stathopoulos, T. (2007). "Turbulent schmidt numbers for cfd analysis with various types of flowfield". *Atmos. Environ.*41, 8091-8099. doi:10.1016/j.atmosenv.2007.06.054

Von Karman, T. (1921). "*On laminar and turbulent friction*". translation by National Advisory Committee for Aeronautics, TM 1092 (originally published in German in 1921)

Von Karman, T. (1930). "*Mechanical similitude and turbulence*". translation by National Advisory Committee for Aeronautics, TM 611 (originally published in German in 1930)

White Frank, M. (1999). "*Fluid mechanics*".

Wilkerson, V.G., and McGahan, J.L. (2005). "Depth averaged velocity distribution in straight trapezoidal channel". *J. Hydr. Engrg.*, 131(6), 509–512. doi:10.1061/(ASCE)0733-9429(2005)131:6(509)

Yang, C.T. (1996). "*Sediment transport theory and practice*". McGraw-Hill Series in Water Resources and Environmental Engineering, Singapore, *ISBN 0–07–114882–5*

Yang, S.Q., and Mc Corquodal, J.A. (2004). "Determination of boundary shear stress and reynolds shear stress in smooth rectangular channel flows". *J. Hydr. Engrg*, 130(5), 458–462. doi:10.1061/(ASCE)0733-9429(2004)130:5(458)